Boundary-Layer Meteorol (2012) 142:55–77
DOI 10.1007/s10546-011-9662-9

ARTICLE

Spatially-Averaged Temperature Structure Parameter Over a Heterogeneous Surface Measured by an Unmanned Aerial Vehicle

A. C. van den Kroonenberg · S. Martin · F. Beyrich · J. Bange

Received: 10 December 2010 / Accepted: 28 September 2011 / Published online: 21 October 2011
© Springer Science+Business Media B.V. 2011

Abstract The structure parameter of temperature, C_T^2, in the lower convective boundary layer was measured using the unmanned mini aerial vehicle M^2AV. The measurements were carried out on two hot summer days in July 2010 over a heterogeneous land surface around the boundary-layer field site of the Lindenberg Meteorological Observatory—Richard-Aßmann-Observatory of the German Meteorological Service. The spatial series of C_T^2 showed considerable variability along the flight path that was caused by both temporal variations and surface heterogeneity. Comparison of the aircraft data with C_T^2 values derived from tower-based *in situ* turbulence measurements showed good agreement with respect to the diurnal variability. The decrease of C_T^2 with height as predicted by free-convection scaling could be confirmed for the morning and afternoon flights while the flights around noon suggest a different behaviour.

Keywords Heterogeneous surface · Spatial averaging · Temperature structure parameter · Unmanned aerial vehicle

1 Introduction

The scattering of electromagnetic and acoustic waves in the atmosphere is affected by the turbulent refractive index field, and can be used to characterize the structure of turbulence in the lower atmosphere (Wyngaard and LeMone 1980). Fluctuations in the refractive index for

A. C. van den Kroonenberg (✉) · J. Bange
Zentrum für Geowissenschaften, Eberhard Karls Universität Tübingen,
Sigwartstr. 10, 72076 Tübingen, Germany
e-mail: aline.van-den-kroonenberg@uni-tuebingen.de

S. Martin
Institute für Luft- und Raumfahrtsystemen, Technische Universität Braunschweig,
Hermann-Blenk-Str. 23, 38108 Braunschweig, Germany

F. Beyrich
Meteorologisches Observatorium Lindenberg/Richard-Aßmann Observatorium,
Deutscher Wetterdienst, Am Observatorium 12, Tauche - OT, 15848 Lindenberg, Germany

electromagnetic radiation are primarily caused by fluctuations in temperature T and absolute humidity Q. This implies that the refractive index structure parameter C_N^2 can be expressed in terms of the structure parameters of temperature C_T^2 and humidity C_Q^2 and the combined structure parameter C_{TQ} (e.g., Wyngaard et al. 1978):

$$C_N^2 = a^2\, C_T^2 + 2\, ab\, C_{TQ} + b^2\, C_Q^2, \tag{1}$$

where a and b depend on the wavelength of the radiation used by the respective system and on environmental conditions such as pressure, humidity and temperature. The temperature fluctuations yield the dominant contribution for electromagnetic radiation at optical wavelengths (i.e. $a^2 \gg b^2$) while the humidity fluctuations are most important in the microwave portion of the spectrum.

Several studies analyzed the behaviour of C_T^2 with height in the convective boundary layer (CBL, e.g., Wyngaard et al. 1971; Coulman 1973), in the marine boundary layer (Fairall et al. 1980), and in the nocturnal boundary layer (Cuijpers and Kohsiek 1989). For thermally unstable atmospheric conditions, Wyngaard et al. (1971) determined a height dependency of $C_T^2 \sim z^{-4/3}$.

For about 15 years, the scintillation method has been applied to measure structure parameters and to derive sensible and latent heat fluxes using scintillometers. These systems operate over a path of between about 100 m and a few kilometres (up to about 10 km) length and therefore provide spatial-averaged turbulence data. Large aperture scintillometers (LAS) were used in many field campaigns over various surface types (e.g. Kohsiek 1982; de Bruin et al. 1995; Nieveen and Green 1999; Meijninger and de Bruin 2000; Meijninger et al. 2006; Hoedjes et al. 2007). The LAS has also been shown to be suitable for continuous long-term turbulence measurements (Beyrich et al. 2002).

While the validity of scintillometer-based surface fluxes has been demonstrated in many studies through a comparison with surface fluxes derived from eddy-covariance measurements, surprisingly little attention has been paid to the validation of the primary scintillometer output parameter: the path-averaged structure parameters, in particular for the LAS. This goal could be achieved by a comparison of C_T^2 measured with a scintillometer at optical wavelengths with turbulence data provided by an in situ measurement system at the height of the scintillometer path. A first approach could be the use of fast-response temperature sensors operated at a tower, however this would still only provide local data. More appropriate would be the performance of in situ measurements with an aircraft just flying along the LAS path. However, conventional research aircraft are not allowed to fly at just a few tens of metres above the ground and their speed is mostly too great to achieve statistically stable results over a path length of just 3–5 km. Small unmanned and automatically operating aerial vehicles (UAV) can provide in situ data at various heights, even very low, over several (ten) kilometres in horizontal distance and also in remote areas. In the field of meteorology, small UAV can, for example, be used to investigate turbulence in the atmospheric boundary layer (ABL), different processes within the stable and convective ABL, and the atmospheric conditions over heterogeneous surfaces. Research UAV are able to probe the lower atmosphere in all spatial directions at any angle with respect to the mean wind. The temporal development of the atmospheric flow can be observed covering the entire depth of the ABL and the lower free atmosphere.

Several UAV systems have already been successfully deployed in field campaigns, such as the robotic plane meteorological sounding system (Ma et al. 2004), the Aerosonde (Holland et al. 2001; Soddell et al. 2004) and the small unmanned meteorological observer (SUMO) (Reuder et al. 2009; Mayer et al. 2010). These are just a small selection of available UAV systems with different payloads used in atmospheric research (e.g. for measurements of

temperature, humidity and pressure). The research UAV system used in our project is in addition capable of measuring the turbulent wind vector and the temperature fluctuations at sufficiently high frequency to calculate the turbulent heat flux. This unmanned meteorological mini aerial vehicle M^2AV was developed at the Technische Universität Braunschweig (TU-BS), and was deployed during several campaigns: LAUNCH-05 (Spieß et al. 2007), Halley-2007 (van den Kroonenberg et al. 2007; van den Kroonenberg 2009), DWD-2007 (van den Kroonenberg et al. 2008) and LITFASS-2009 (Martin et al. 2011).

The focus of the paper is the spatially-averaged temperature structure parameter measured by the M^2AV in comparison with tower data and the scaling proposed by Wyngaard et al. (1971). To do so, C_T^2 was calculated from in situ airborne measurements along straight and levelled flights (legs) and from tower-based sonic anemometers and thermometers at several altitudes. The experiment was performed on two hot summer days (11 and 12 July, 2010) in the daytime CBL over a fairly flat but heterogeneous landscape near the Meteorological Observatorium Lindenberg.

The main research questions of the study are:

1. Is the M^2AV able to determine reliable values (i.e. with acceptable systematic and statistic errors) of the spatially-averaged C_T^2 from fast-response temperature measurements along flight legs of 3–5 km length over a heterogeneous land surface?
2. Can the leg-averaged C_T^2 measured by the M^2AV at different heights be confirmed by time-averaged point measurements of C_T^2 at a meteorological tower?
3. Does the heterogeneous terrain affect the spatial variability of the temperature structure parameter significantly, at a typical installation height of an optical scintillometer?
4. What is the height dependence of C_T^2 in the convective ABL over a heterogeneous surface? Does it agree with the free-convection scaling as proposed by Wyngaard et al. (1971)?

2 Theory

The structure parameter of temperature

$$C_T^2 = D_T(r)\, r^{-2/3}, \tag{2}$$

is a proportionality factor in the 2/3-law expression (Kolmogorov 1941) for the structure function and is only valid within the inertial subrange of locally isotropic turbulence (Wyngaard et al. 1971). The structure function $D_T(r)$ of temperature is defined by

$$D_T(r) = \frac{1}{N-n} \sum_{i=1}^{N-n} \left[T(x_i) - T(x_i + r)\right]^2, \tag{3}$$

for a certain data record where N denotes the number of data points in the record, x is the spatial coordinate, $r = r(n)$ is the spatial displacement (lag), and n is the number of data points associated with lag r. The structure function can also be calculated using the variance σ_T^2 and the covariance function Cov_T or the autocorrelation function ϱ_T, respectively

$$D_T(r) = 2\left[\sigma_T^2 - \mathrm{Cov}_T(r)\right] = 2\,\sigma_T^2\left[1 - \varrho_T(r)\right], \tag{4}$$

which is only valid for homogeneous turbulence. The combination of (4) and (2) shows that an increase of the temperature variance σ_T^2 results in an increase of the calculated C_T^2. Since most of the available software libraries use Fourier transformations to calculate the

covariance function (and thus induce systematic errors due to improper data windowing), we used (3) to calculate $D_T(r)$.

The structure parameter C_T^2 is calculated from in situ data using the structure function (3) within the inertial subrange. The inertial subrange of quasi-isotropic turbulence typically lies between scales of a few millimetres to a few hundred metres. The lower limit represents the transition to the dissipation range where the turbulence decays. These small scales could not be resolved by our temperature sensors due to the limited sensor response that caused the lower limit $r_{\min}$ of the measured inertial subrange. The upper limit $r_{\max}$ represents the transition to the production range, which depends on the height of the boundary layer, the thermal stratification and on the distance to the ground (or the nearest stably stratified layer, Lumley and Panofsky 1964). The precise position of the upper limit $r_{\max}$ in a power spectrum or structure function is difficult to predict. However, the integral scale I might be a suitable indicator. Although I is not a direct measure for the upper limit, it represents the outer or macro scale of a turbulent quantity (Rotta 1972). The associated integral time scale can be interpreted as the correlation time, the persistence or memory of the turbulent flow (Kaimal and Finnigan 1994). In general it can be assumed that the integral scale is smaller than the upper limit of the inertial subrange, $I < r_{\max}$. The integral time scale I_T for temperature T is defined by

$$I_T = \int_0^{\tau_1} \mathrm{d}\tau \frac{\left\langle T'(t+\tau)T'(t)\right\rangle}{\left\langle T'^2\right\rangle} = \int_0^{\tau_1} \mathrm{d}\tau \frac{\mathrm{Cov}_T(\tau)}{\sigma_T^2}, \tag{5}$$

and is calculated by integration from zero lag to the first zero crossing at τ_1 (Lenschow and Stankov 1986). The transformation into the integral length scale is carried out by multiplication of the integral time scale by the aircraft's ground speed, or, considering tower measurements, by the mean wind speed, assuming that Taylor's hypothesis of frozen turbulence is valid.

2.1 Maximum Record Size

The temperature structure parameters were determined from fast temperature measurements T under the assumption that Taylor's hypothesis of frozen turbulence is fulfilled. That is, the measurement period of one data record has to be shorter then the time needed for the turbulence to develop. A measure of the convective time scale is the large-eddy overturning time (Sorbjan 2005; Bange et al. 2007):

$$\tau_* = \frac{z_i}{w_*}, \tag{6}$$

with the boundary-layer height z_i and the convective velocity w_*,

$$w_* = \left[\frac{g}{\bar{\theta}}\, z_i\, \left\langle w'\theta'\right\rangle_0\right]^{1/3}, \tag{7}$$

where the buoyancy parameter is $g/\bar{\theta}$ and the kinematic surface heat flux is $\left\langle w'\theta'\right\rangle_0$. To fulfill Taylor's hypothesis of frozen turbulence the measurement period should not exceed the large-eddy overturning time.

2.2 Minimum Record Size

The following analysis of the influence of surface heterogeneity on the turbulent structure requires the calculation of the structure function along smaller flight sections (so-called sub-legs of length W). In order to define a minimum length of these sub-legs, it is helpful to calculate the statistical error of (3) as a function of the sub-leg length i.e. the number N of data measured along the sub-leg. In order to estimate the statistical error of the structure function we regard (3) for a fixed lag $r(n)$ as an average of the data series

$$d_i(n) = [T(x_i) - T(x_i + r(n))]^2, \tag{8}$$

such that

$$D_T(r) = \frac{1}{N-n} \sum_{i=1}^{N-n} d_i(n) = \overline{d(n)}, \tag{9}$$

where the overbar denotes the average over $N - n$ realisations of $d(n)$. Now, the statistical standard error of such an average is defined by

$$SE_{\overline{d(n)}} = \frac{\sigma_{d(n)}}{\sqrt{N-n}} = SE_{D_T(r)} \tag{10}$$

and can be, due to (9), identified with the standard error $SE_{D_T(r)}$ of the structure function (3) for a certain lag $r(n)$. The standard error (10) is a function of the data size N of the sub-leg, the lag n, and the standard deviation $\sigma_{d(n)}$ of data series $d_i(n)$ in (8). It can be expected that $\sigma_{d(n)}$ increases first with N (as long as N is too small to provide a significant record of $d(n)$), and then (for larger record sizes N) decreases towards a limit. From (10) it can be expected that the standard error of the structure function will increase while the record size is not significant, and will decrease $\sim(N-n)^{-1/2}$ for larger record sizes N. The first two criteria for a minimum sub-leg length are therefore

C1 The record size N has to be large enough to ensure that $\sigma_{d(n)}$ decreases towards a limit for increasing N.

C2 The record size N must be large enough with the relative standard error $SE_{D_T(r)}/D_T(r)$ below a certain threshold (e.g. 10%).

The third criterion is based on the sizes of the turbulent eddies:

C3 In order to measure all scales within the complete inertial subrange, the length $W(N)$ of the sub-legs (with record size N) should be larger than the integral length scale. To gain better statistics for these scales, W should be at least twice the integral length scale, $W \approx 2I$.

3 Data

A 2-day field campaign was carried out on 11 and 12 July 2010, at and around the GM Falkenberg (where GM stands for boundary-layer field site) of the German Meteorological Service (where GM stands for the German word “Grenzschichtmessfeld”, which means “boundary-layer field site”) of the Meteorological Observatory Lindenberg—Richard-Aßmann-Observatory (MOL-RAO) of the German Meteorological Service (Deutscher Wetterdienst, DWD). This field site is situated about 5 km to the south of the observatory in a rural landscape in eastern Germany (e.g. Beyrich and Mengelkamp 2006). During the campaign, the lower part

Table 1 The evolution of the ABL height (m) as determined from the radiosoundings

Time (UTC)	11 July	12 July
0445	200	210
1045	1870	2120
1645	2740	2330

of the ABL was probed by a large-aperture scintillometer (LAS), a sodar-RASS, a 99-m tower and by a M^2AV. In addition, four radiosondes were launched daily at the MOL-RAO at around 0445 UTC, 1045 UTC, 1645 UTC and 2245 UTC, respectively. On the tower, two eddy-covariance (EC) systems (USA-1 sonic anemometer USA-1, METEK GmbH, and infrared gas analyzer LI7500, LiCor Inc.) were installed at heights of 50 m and 90 m to perform wind, temperature and humidity fluctuation measurements. The LAS was installed over a pathlength of 4.8 km between the GM Falkenberg and MOL-RAO sites at an effective height of 43 m above ground. Except for the M^2AV system, all measurement systems were part of the MOL-RAO operational measurement program.

The M^2AV performed a series of flights around the tower and along the LAS path at different heights and during different times covering the daytime evolution of the convective ABL. The present analysis is focusing on the M^2AV and EC measurements; the discussion of the LAS data will be the subject of a separate study. The weather at the field site on 11–12 July 2010, was influenced by an anticyclone located over the Baltic States, and was dominated by a cloud-free sky with afternoon and temperatures rising to 38°C. The wind direction during the first day remained constant between 140° and 180° with a wind speed at 10 m that increased from 2 to 5 m s^{-1} during the day. During the second day of the campaign (12 July 2010) the wind direction changed from 110° in the morning (0800 UTC) towards 190° in the afternoon (1500 UTC); the wind speed at 10 m increased from 2 to 5 m s^{-1}, and the wind became very gusty at midday. The maximum daytime sensible heat fluxes (typical values for this area as measured by surface stations) varied between 130 W m^{-2} over evaporating surfaces (with Bowen ratio ≈ 0.6), about 180 W m^{-2} over dried farmland surfaces (Bowen ratio ≈ 1) and up to 500 W m^{-2} over the pine forest (Bowen ratio between 5 and 10). The ABL height was determined from the MOL-RAO operational radiosoundings with daytime values listed in Table 1.

3.1 Sonic Anemometer

The sonic anemometer of type USA-1 from METEK GmbH have a pathlength of 0.175 m, and were used to measure the wind components and the acoustic temperature at a 20 Hz sampling rate.

The velocity of sound is derived by the travelling time of the short pulses of ultrasonic sound, which is exchanged in three different directions between pairs of sound probes. This sound velocity is composed of the sound propagation of the air at rest and the wind speed parallel to the three trajectories of the pulses. The three-dimensional wind vector is determined by combining the sound velocities of the three propagation directions, while the acoustic temperature (T_s) is derived from the sound velocity in a motionless atmosphere. The speed of sound is basically a function of temperature, but additionally it depends on atmospheric humidity. Therefore, the acoustic temperature exhibits a small dependence on humidity (water vapour pressure e) as well. The relation between air temperature (T_a) and acoustic temperature is described by

$$T_s = T_a \left(1 + 0.32 \frac{e}{P}\right), \tag{11}$$

where P is atmospheric pressure (see, e.g. Kaimal and Gaynor 1991). For the conditions during the experiment (with daytime temperatures of up to 38°C and a daytime water vapour pressure of 12–15 hPa) this water vapour contribution to the absolute value of temperature is smaller than 1%. However, for the derivation of C_T^2 we rely on temperature differences. For a single temperature difference value between two parcels of air the error introduced is of the order of $0.32 T_a \Delta e / P$ where Δe is the water vapour pressure difference between the two air parcels. Assuming Δe to be smaller than 0.5 hPa we estimate a resulting error in C_T^2 of about $1–2 \times 10^{-3}$ K^2 m$^{-2/3}$, corresponding to about 5–20% of the C_T^2 values during daytime. We consider this as an acceptable value taking into account the variability of the temperature structure parameter over several orders of magnitude in its diurnal cycle.

The complete EC systems (sonic anemometer and infrared gas analyzer) were mounted on booms of 5 m length, mounted on the western side of the tower and pointing towards south. This ensured undisturbed measurements at wind directions between about 90° and 300°.

3.2 Meteorological UAV

The M^{2}AV is a twin-engine member of the Carolo family of automatically operating mini-UAV, constructed by the Institute of Aerospace Systems of the TU-BS. The UAV has a wing span of 2 m and a maximum take-off weight of 6 kg. The aircraft operates at a mean true airspeed of 22 m s^{-1} and measures the meteorological and navigation data at 100 Hz. The meteorological sensor package consists of a 5-hole probe, an inertial navigation unit and a GPS receiver for measuring the wind direction and speed (with an inverse time response of 30 Hz), a Vaisala HMP 50 for temperature and humidity measurements (1 Hz), and a thermocouple (self-made) for measuring the fast temperature fluctuations (10 Hz) (van den Kroonenberg et al. 2008; Martin et al. 2011).

For this study, measurements of fast temperature fluctuations were essential. To obtain a fast-response and low-cost sensor, the thermocouples were self-developed and manufactured in-house. The wire used for the thermocouple of type K (NiCr–Ni) had a diameter of 0.13 mm, resulting in a fast sensor-response time. The cold-junction compensation was realised with a LM35 temperature sensor. Since the temperature signal measured with the thermocouple showed a drift in time, it was only used to measure the high-frequency temperature fluctuations. Additionally, the Vaisala HMP 50 measured the air temperature (resistance thermometer) with an accuracy of about ±0.6 K but with a slow response time of about 1–2 s in flight. This sensor provided long-term stability and high accuracy. For the final temperature determination the HMP 50 (low frequencies) was combined with the signal of the thermocouple (high frequencies) by complementary filtering with a cut-off frequency of 0.02 Hz. This filter was based on the Savitzky-Golay filter (Bromba and Ziegler 1981), which has a low-pass characteristic with flat pass-band.

To operate the M^{2}AV a thorough preparation was necessary. For every UAV campaign the operator has to apply for flight permission from the aeronautical authority that is responsible for the experimental area. For the 2010 campaign flight permission was obtained with the following restrictions: 1. No flights above 1500 m, 2. No flights after sunset and before sunrise, and 3. Only flights within sight to be able to operate the UAV manually in case of other aircraft approaching. The UAV was operated by the autopilot during flight but take-off and landing were performed by a human pilot who was also supervising the flight mission as safety pilot. In Germany UAV flights out of sight are currently not permitted. Therefore flight legs longer than 3 km have to be supervised by additional safety pilots. Regarding the flight performed during July 2010 three pilots were necessary for supervision of the whole M^{2}AV flight paths. The coordinator of the flight campaign was responsible for establishing

Table 2 All horizontal subsections within one M^{2}AV flight in chronological order with the start and end points as indicated in Fig. 1

Name	Direction	Distance (km)	Start–end	Height (m, day 1)	Height (m, day 2)
leg01sn	North	3.3	B–A	60	60
leg01ns	South	5.6	A–D	60	60
leg02sn	North	5.6	D–A	80	90
leg02ns	South	5.6	A–D	100	90
box03	n–w–s–e	2.0	D–D (4 legs)	100	100
leg04sn	North	3.3	B–A	60	60
leg04ns	South	5.6	A–D	60	60
box05sn	North	2.0	D–C	70	100

the flight strategies, monitoring the ground control station and the data post-processing. The flight strategies were planned using the ground-control station and the actual flight paths were sent to the aircraft before take-off. During flight changes of waypoints were possible when the UAV was flying within the telemetry range. So far meteorological data were not sent to the ground station as this feature was not available at the time of the campaign. Thus, the data were stored on-board on memory cards and post-processing was done subsequently.

3.3 Flight Strategy

Each M^{2}AV flight was divided into horizontal subsections that are listed in Table 2. One flight of about 40 min consisted of one square pattern around the tower at 100 m above the ground and seven legs along the scintillometer path, passing the tower, at different heights (Fig. 1). On the first day, July 11, these legs along the scintillometer path were flown at 60, 70, 80 and 100 m above the ground; the first flight started at 0504 UTC and the last flight ended at 1756 UTC (local summer time was UTC + 2 h). On the second day, July 12, the long legs parallel to the scintillometer path were flown at 60, 90 and 100 m above the ground. The first flight on the second day started at 0613 UTC and the last flight ended at 1743 UTC. In the following the longer flight-sections in the north or south directions are named as ‘leg’ and the five shorter sections that are part of the square pattern around the 99-m tower are named as ‘box’.

4 Methods

The temperature structure parameters discussed above were determined by two kinds of systems, the M^{2}AV and sonic anemometers mounted on a tower, under the assumption that Taylor’s hypothesis of frozen turbulence is fulfilled. Therefore the measurement period of one record has to be shorter than the time needed for the turbulence to develop, which is again related to the large-eddy overturning time (see Eq. 6).

To calculate τ_*, data from the radiosoundings ($\bar{\theta}$ and z_i) and several ground stations ($\langle w'\theta' \rangle_0$) were used. The values of the large-eddy overturning time for both the measurement days (11 and 12 July 2010) were about 10 min in the morning (0500 UTC) and increased to 15–20 min in the afternoon (1700 UTC). As the aircraft needed up to 4 min for the longest flight legs, the turbulence was considered frozen and the captured time series could therefore

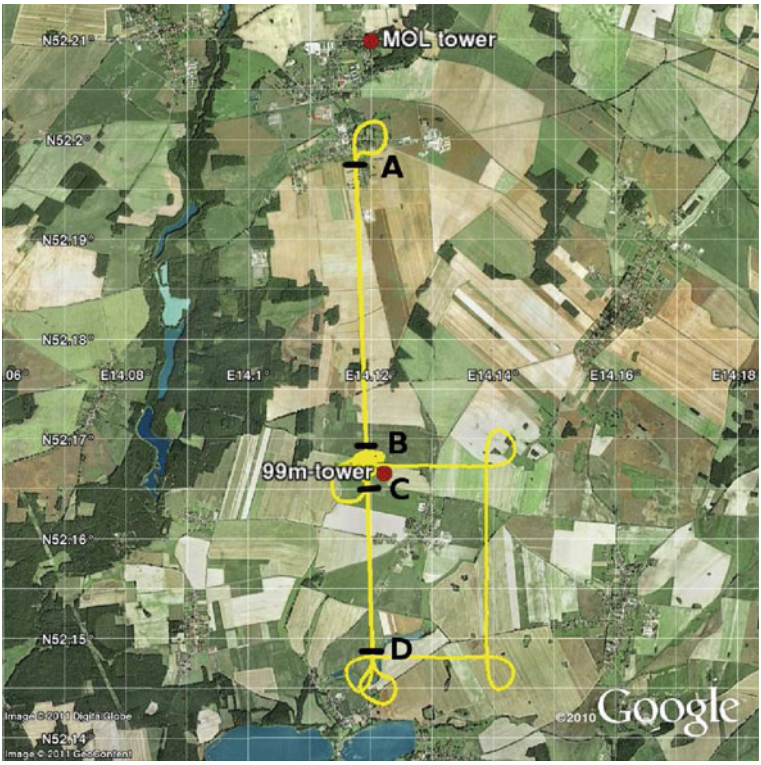

Fig. 1 M^2AV track during the campaign (*yellow line*) with the 99-m tower in Falkenberg and the MOL tower in Lindenberg marked as *red dots*. The letters A, B, C and D indicate the start and end points of the flight legs listed in Table 2. *Source*: "DWD boundary-layer field site". 52.1785°N and 14.1298°E. *Google Earth*. October 7 2005; November 29 2010

be regarded as a spatial series. The spatial series was obtained by multiplying the measured time series with the aircraft ground speed. In the case of the sonic anemometer, the turbulence was considered frozen because the data were recorded within 10-min periods. The measured time series (10-min records) were transformed into a spatial series by multiplication with the mean wind speed. The difficulty of comparing the data of both systems is mainly based on these different measuring characteristics. Additionally, both systems see a different footprint area, resulting in a different relative contribution of the various land-use types to the signal measured at the tower and along the flight path, respectively.

4.1 Determination of C_T^2 from UAV Data

The structure function $D_T(r)$, with spatial lag r, was calculated from straight and level flights (legs). Figure 2a shows an example of the normalized structure function according to (Eq. 2) measured by the UAV. The shaded area represents the standard error (10) of the structure function normalized by $r^{-2/3}$. The inertial subrange is shown as a horizontal plateau defined between the two boundaries, $r_{\min}$ and $r_{\max}$. The decrease of the structure function for lags smaller than $r_{\min}$ was caused by the time response of the temperature sensor, which was 0.1 s corresponding to a minimum spatial resolution of 2.6 m (at a ground speed of 26 m s^{-1} as

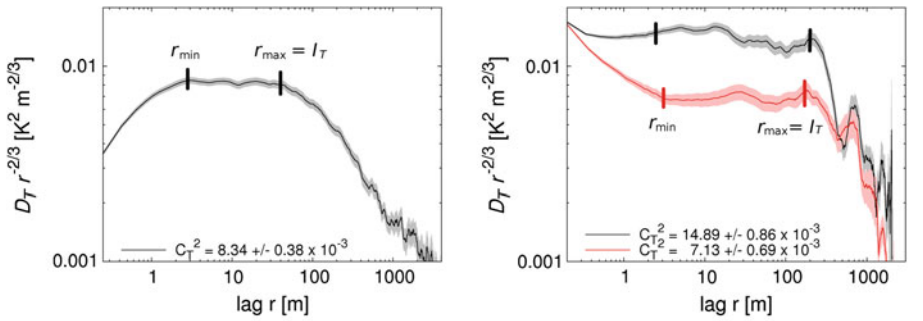

(a) UAV data obtained at 90 m.

(b) Sonic at 50 m (black line) and at 90 m (red line).

Fig. 2 Examples of the normalized structure functions $D_T(r)r^{-2/3}$ (2) (*solid lines*) and their standard error (*shadings*) according to Eq. 10 calculated from the temperature measurements of 12 July around 0750 UTC. The structure functions are used to determine C_T^2 between the boundaries $r_{\min}$ and $r_{\max}$. These mean C_T^2 values are shown in the legend for all three data records

achieved for the flight analyzed in Fig. 2a). For all the UAV legs flown during the campaign (11 and 12 July, 2010), this lower boundary $r_{\min}$ varied due to the changing ground speed mainly between 1.8 and 2.6 m. The upper boundary $r_{\max}$ was assumed to be larger than the integral scale, $r_{\max} > I_T$. Nevertheless, I_T was used as a measure for this upper boundary. The integral length scale of temperature I_T for this example was 40 m, and for all the UAV legs, I_T varied between 25 and 165 m.

Based on these two boundary estimates a section representing the inertial subrange for all legs was defined between $r_{\min} = 2.5$ m and $r_{\max} = 25$ m, and the mean C_T^2 calculated within this range. The standard error of the mean C_T^2 was defined at the largest scale of the inertial subrange at $r = 25$ m, using

$$SE_{C_T^2} = SE_{D_T(r)}\, r^{-2/3}. \tag{12}$$

4.1.1 Spatial Series of C_T^2 Along the Flight Path

The spatial series of C_T^2 were calculated by using a moving window with length W within which the structure function $D_T(r)$ was computed. This window was defined for each data point i of the temperature spatial series with i as the centre point. By moving this window the semi-local temperature structure parameter $C_T^2(\mathrm{i})$ was calculated. This resulted in C_T^2 values typically every 0.22 m (equivalent to 0.01 s with a 100 Hz sampling rate and 22 m s^{-1} typical ground speed), which were based on temperature data over the distance W.

The procedure on how to define the window length will be explained using one example: a 5.6 km long leg at 60-m height performed on July 11 around 1052 UTC. Figure 3 (lower panel) shows the C_T^2 spatial series that was calculated for this example by using four different window lengths: 10, 15, 20 and 30 s, which correspond to 220, 330, 440 and 660 m, respectively. The upper panel shows the temperature series measured during that leg that gives information on the temperature fluctuations in relation to the calculated C_T^2.

The appropriate window size should be short enough to resolve the surface heterogeneity of the landscape. The smaller field sizes in the experimental area are between 200 and 400 m. To resolve these surface-related scales the optimum window length should be as small as

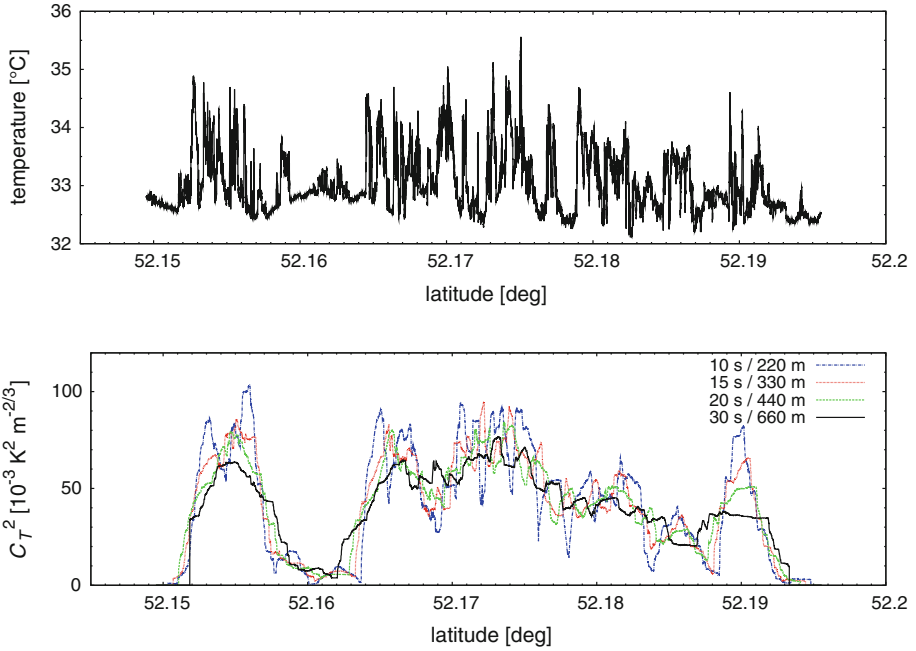

Fig. 3 Example of the measured temperature (*upper panel*) and the corresponding spatial series of C_T^2 (*lower panel*) measured on 11 July around 1052 UTC. *Lower panel*: the different *lines* represent the different length W over which C_T^2 is calculated

200 m or at least not larger then 400 m. The three criteria mentioned at the end of Sect. 2 are now defined more precisely:

C1 It was found that $\sigma_{d(n)}$ (10) decreased towards a limit for record sizes N larger than 800. Thus, the record size must be larger than 800 data points (equivalent to 180 m) to provide a significant structure function.

C2 The standard error of the calculated C_T^2 decreases for more data points and should be around or less than 10%.

C3 The largest calculated I_T for all the legs was 165 m ($N = 750$). To be certain of including all the scales within the inertial subrange a minimum sub-leg of $N = 2I = 1500$ was chosen.

Considering these criteria, a window length with 1500 data points corresponding to 330 m was chosen for all the flights. The standard error for the example shown in Fig. 3 with $N = 1500$ is 11.8%, which we considered as acceptable (according to C2).

4.2 Determination of C_T^2 from Sonic Data

The time series of the temperature structure parameter was created by calculating C_T^2 within a moving window. One of the objectives was to compare the leg-averaged C_T^2 of the M^{2}AV to the sonic measurements. Therefore the size of the window was defined as the time needed for an air parcel passing the sonic to move over a distance comparable to one flight leg (3–5 km). The wind speed (at measurement height) varied between 2 and 6 m s^{-1} during daytime on both measurement days (11 and 12 July 2010). A time window of 10 min was chosen, which

corresponds to a distance of 2.4 km, considering a mean horizontal wind speed of 4 m s^{-1}. To ensure that Taylor's frozen turbulence theory is valid, this time window must not exceed the eddy overturning time (see Eq. 6), which was around 10 min in the morning and increased to 15–20 min in the afternoon. At least the calculated τ_* was equal or slightly larger than the chosen window size. If an even smaller window size was chosen, the objective to compare the leg-averaged data of the M^2AV with the sonics would not be achieved.

The same method as for the UAV was used to determine the C_T^2 values from the calculated structure functions. Figure 2b shows an example of the normalized structure function according to (2) measured by both sonics. The inertial subrange was identified by the estimation of the two boundaries $r_{\min}$ and $r_{\max}$. The increase of the structure function towards the smaller lags ($<r_{\min}$) corresponded to a horizontal tendency of the variance spectrum at the high frequencies (not shown here), due to noise and the limited temperature resolution of the sensor (which was 0.025 K). The lower limit $r_{\min}$ was affected by this limited temperature resolution and the size distribution of the turbulent eddies in the measured flow. During the daytime the $r_{\min}$ determined from both sonics varied between 1 and 3 m.

The integral length scales of temperature for both sonics varied mainly between 25 and 200 m (calculated over a 10-min time interval). No significant difference between the two sonics (response time and outer scales) was observed. Based on these boundaries, the inertial subrange for all the 10-min periods was defined between $r_{\min} = 3$ m and $r_{\max} = 25$ m. Within this range the mean C_T^2 value was calculated and the standard error of C_T^2 (see Eq. 12) was calculated for $r = 25$ m.

5 Results

5.1 Diurnal Cycle

The spatially-averaged C_T^2 was determined according to (2) for each flight leg (see Appendix: Tables 3, 4). The temperature time series measured by the two sonic anemometers were used to compute the tower-based C_T^2 values. The flow was roughly from the south on both days, which resulted in a footprint for the sonic measurements located south of the tower. Figure 4 shows the time series of the 10-min averaged C_T^2 values calculated from the sonic data compared to the spatially-averaged C_T^2 values derived from the M^2AV measurements. No C_T^2 value could be determined from the sonic measurements before 0600 UTC and after 1600 UTC, since the sonics were not able to resolve temperature differences smaller than 0.025 K. During these periods, the measurements did not show the expected inertial sub-range ($r^{-2/3}$), which indicated that the turbulent fluctuations were too small to be resolved.

Although both systems measured different footprint areas, the derived C_T^2 values were in the same order of magnitude. In the morning and in the afternoon, both systems agreed well, but around noon the UAV gave higher C_T^2 values. Both systems showed at all altitudes a clear diurnal cycle with an increasing C_T^2 after sunrise (0256 UTC), the highest values occurring around solar noon (1109 UTC) and a decreasing C_T^2 towards sunset (1921 UTC).

Since the temperature variance decreases with height, also the temperature structure parameter decreases with height (see Eq. 4). This was measured by both systems during both days except in the early morning (before 0600 UTC) of July 11. The fact that during this one flight the C_T^2 values increased with height will be analyzed in more detail in Sect. 5.2.

As the M^2AV measured an increasing C_T^2 in time, also the variability between the different flight legs at a given altitude increased. During noon, the turbulent eddies were intense and large, which resulted in large temporal fluctuations. These large temporal fluctuations

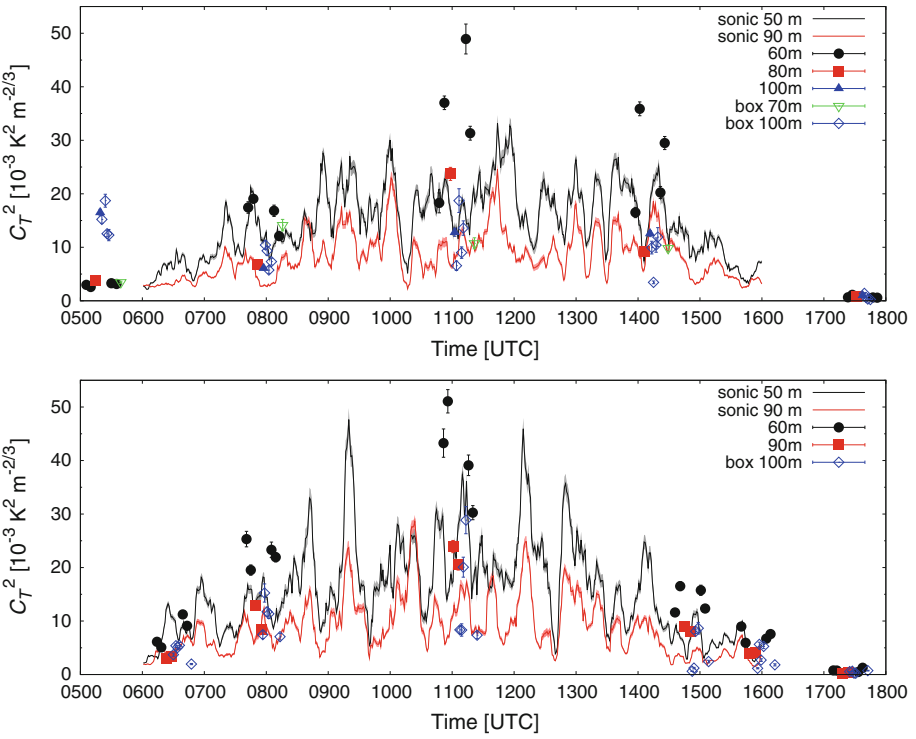

Fig. 4 The diurnal cycle of C_T^2 measured on July 11 (*upper panel*) and July 12, 2010 (*lower panel*). The *symbols* represent the spatially-averaged C_T^2 measured by the M^{2}AV at different heights with their standard error indicated by the error bars. The *solid lines* represent the time series (using a moving window of 10 min) derived from the sonics with the standard error of C_T^2 (12) represented by the *filled area*

caused an unsteady convective flow in which more repeated flight legs should be performed to obtain statistically significant C_T^2 values. The large variability of the data at the lowest flight level around noon indicated that four repetitions of the flight leg were probably not enough to achieve statistical significance. Nevertheless, we attempted to quantify this variability to describe the tendency during the day. A measure of this variability is the calculated standard deviation of the mean C_T^2 from the four flight legs at 60 m. For the first day, this standard deviation increased towards midday to 11.0×10^{-3} K^2 m$^{-2/3}$, which is larger than the statistical standard error of 1.8×10^{-3} K^2 m$^{-2/3}$ for these legs. On the second day, the standard deviation was also largest for the midday flight (around 1100 UTC), 7.5×10^{-3} K^2 m$^{-2/3}$ and was again larger then the mean standard error of 2.0×10^{-3} K^2 m$^{-2/3}$ for these legs. Besides this, the standard deviation with respect to the mean C_T^2 also increased towards midday reaching values of 33 and 18% for 11 and 12 July, respectively. This variability of the structure parameter corresponded to a large variability between the measured turbulent heat fluxes on these lower flight legs (not shown here) that should be expected for such short flight distances of 5.6 km and less (see also Lenschow and Stankov 1986; Lenschow et al. 1994). The variations of the 10-min sonic values at 50 m (over 1 h) were in the same order of magnitude as the leg-to-leg variability of the UAV in 60 m. These variations measured by the sonic were reduced at 90 m by as much as 50%.

The M^{2}AV flights in the late afternoon (after 1700 UTC) showed very small C_T^2 values. During this time period the transition between the daytime convective ABL and the nocturnal

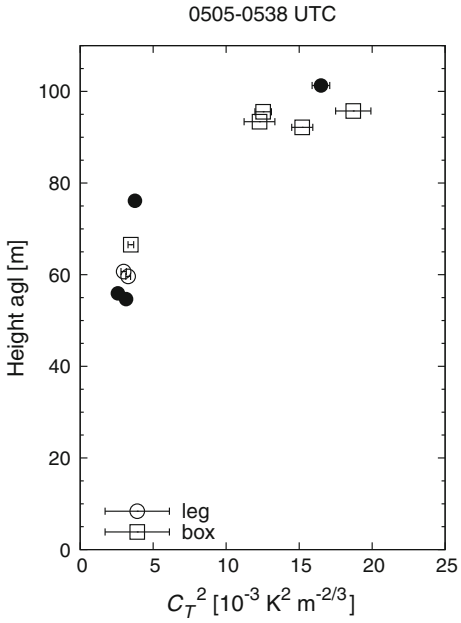

Fig. 5 Vertical profile of C_T^2 measured on July 11 by the M^{2}AV during the first flight between 0505 and 0538 UTC. The M^{2}AV short legs (*open black circle*), the long legs (*closed black circle*) and the box flight (*open black square*) are shown

stable ABL was in progress. The late afternoon transition process normally starts a couple of hours before sunset (which was at 1921 UTC) and is characterized by decaying turbulence. This weak (residual) turbulence in the ABL resulted in the very low C_T^2 values also characterized by no significant height dependency.

5.2 Early Morning Increase of C_T^2 with Height

During the first flight on 11 July the M^{2}AV measured relatively high C_T^2 values at 100 m compared to the lower levels. On the second flight, which was performed almost 3 h later, the expected decrease of C_T^2 with height was found (Fig. 4 upper panel; Appendix Table 3). Figure 5 clearly shows the strong increase of C_T^2 with height between 80 and 90 m above the ground measured during the first flight. This increase was an indication that the large C_T^2 values at 100 m were not due to turbulence produced at the surface but resulted from turbulence generated aloft.

We see two possible processes that might have caused the enhanced C_T^2 values aloft: turbulence in the shear zone of a (decaying) low-level jet (LLJ) and/or entrainment processes at the top of the shallow growing mixed layer. There are indications for both in the data: the 2245 UTC radiosounding ascent, released at MOL, showed a strong wind shear of 0.048 s^{-1} just below the wind-speed maximum of 12 m s^{-1} at 220 m (Fig. 6). This phenomenon is known as a nocturnal LLJ. These LLJs develop under moderate synoptic pressure gradients, and the wind in the surface layer can be very weak but the wind aloft can become supergeostrophic and decrease again at higher levels (e.g. Thorpe and Guymer 1977; Banta et al. 2002; Cuxart 2008). The strong shear below and above the LLJ wind maximum can cause turbulent mixing in these layers (Cuxart and Jiménez 2007). This LLJ is a common feature for the experimental area. Görsdorf et al. (2004) report an occurrence frequency of around 10% based on an analysis of wind profiles synthesized from sodar and wind profiler measurements over three years (with maxima in spring and autumn).

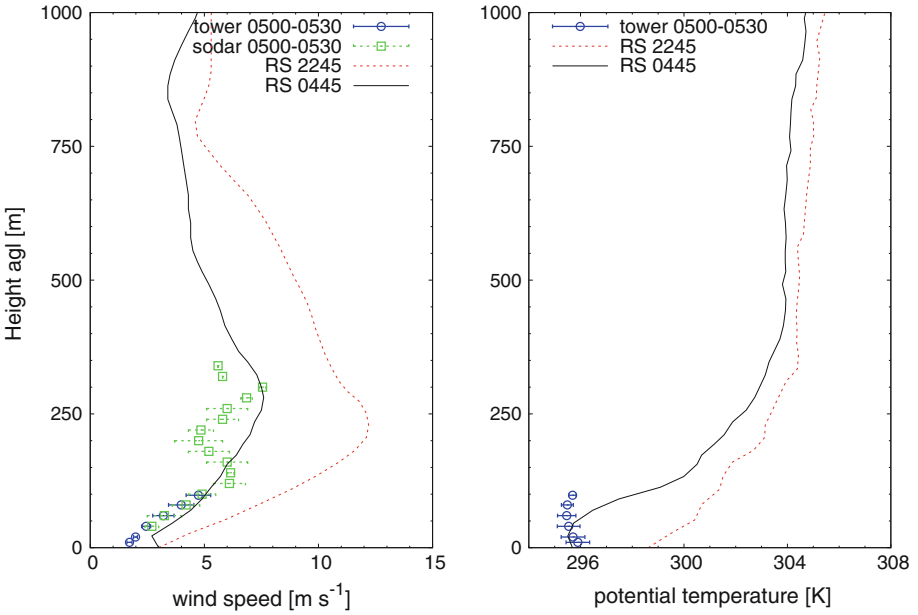

Fig. 6 Radiosoundings at MOL, tower and sodar measurements at Falkenberg. *Left*: vertical profile of the wind speed, *right*: vertical profile of the potential temperature. The *dashed red line* represents the 2245 UTC ascent, the *solid black line* the 0445 ascent, the *blue circles* represents the tower measurements and the *green squares* represent the sodar measurements in the time period between 0500 and 0530 UTC

The 0445 UTC radiosonde was released almost two hours after sunrise (sunrise was at 0256 UTC). The LLJ measured during the 0445 ascent was weaker but still significant with a wind maximum of 7.5 m s^{-1} at 280 m and a wind shear of 0.02 s^{-1} just below this maximum. The strong wind shear measured by the radiosonde was confirmed by the sodar and the tower measurements (between 0500 and 0530) up to 120 m.

The temperature profiles measured on the morning of July 11 are shown in Fig. 6 (right panel): The radiosonde ascent from 0445 UTC shows a very shallow mixing layer up to about 50 m above ground and a large temperature increase between 50 and 150 m. During the time of the flight, the depth of the shallow mixing layer grew beyond the tower range. While the tower temperature profile shows increasing values above 60 m until 0520 UTC, the temperature decreases or remains almost constant up to 100 m later. Moreover, the CBL depth estimated from the backscatter intensity profiles of the sodar operated at GM Falkenberg increased from 100 to 120 m during the time of the flight. Both observations indicate that the morning flight on July 11 took place in the upper part of a growing shallow convective mixing layer, where entrainment of warm air from aloft is known to produce enhanced values of the temperature structure parameter (e.g., Frisch and Clifford 1975; Fairall 1987; Braam 2010).

On the second flight day, the soundings also showed a strong LLJ at 2245 UTC (figure not shown here) but this LLJ decayed out before the second sounding at 0445 was released. The 0445 UTC sounding showed a constant wind speed of 2 m s^{-1} close to the surface and aloft. As a result, the measured C_T^2 values during the first flight (0630 UTC) showed the expected decrease with height and no high values of C_T^2 were measured at 100 m.

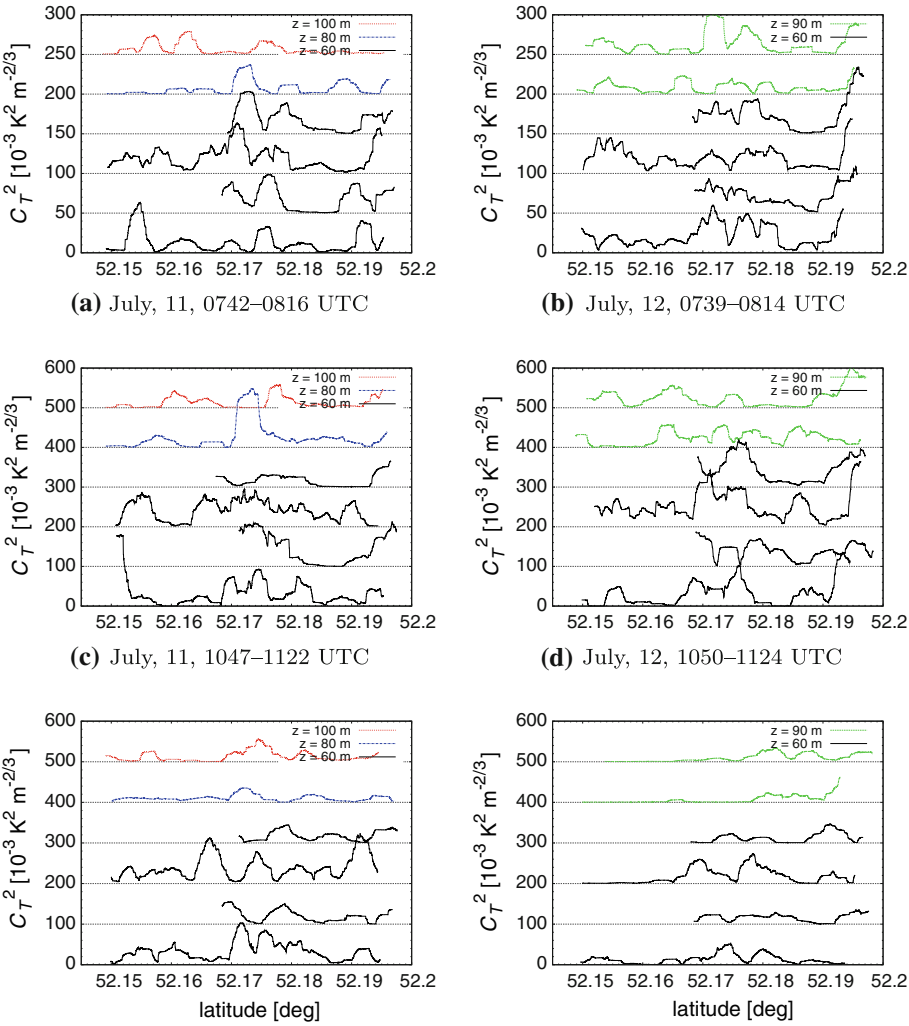

(a) July, 11, 0742–0816 UTC **(b)** July, 12, 0739–0814 UTC

(c) July, 11, 1047–1122 UTC **(d)** July, 12, 1050–1124 UTC

(e) July, 11, 1356–1430 UTC **(f)** July, 12, 1435–1509 UTC

Fig. 7 The C_T^2 spatial series of all the straight legs in the north–south direction (flight distance of 3.3 or 5.6 km). The C_T^2 values were computed with a moving window of length 330 m. The spatial series are displayed each with an offset of 50×10^{-3} K^2 m$^{-2/3}$ (**a**) and (**b**) or 100×10^{-3} K^2 m$^{-2/3}$ (**c**)–(**f**) to the spatial series below. The different colours represent the different flight-levels: *black solid line* 60 m, *blue dashed-dotted line* 80 m, *green dashed line* 90 m and the *red dotted line* 100 m

5.3 Heterogeneity of C_T^2 Along the Flight Path

It was observed that particularly during midday, at the lowest flight levels, C_T^2 varied significantly between the individual legs (Fig. 4). We assume that these variations in the turbulent field were due to two effects: (1) The structure of turbulence which varied in time and space, and (2) The heterogeneity of the surface which caused variations in space. To analyze the turbulence-related and the surface-related effect in more detail, the spatial series of C_T^2 along the flight path are shown in Fig. 7. The data are plotted with an artificial offset on the C_T^2

value for better visibility and distinction between the different legs. The panels on the left represent three consecutive flights on 11 July, and the Figures on the right represents three flights on 12 July. The spatial series show an irregular behaviour of the temperature structure parameter. The magnitude of C_T^2 was highest for the flights around solar noon (1109 UTC), which was caused by strong convection. The flights at 60 m consistently show strong variation (peaks) between a latitude of 52.17° and 52.18°, which then was followed (in the northward direction) by a decrease of C_T^2. At the northern end of the legs, at latitude 52.19°, C_T^2 increased again. Compared to the lowest flight level (60 m) the C_T^2 values at 80, 90 and 100 m were lower and the development in space was more regular. Nevertheless, the peaks between 52.17° and 52.18° can also be identified at these higher flight levels. On the first flight day, the individual C_T^2 peaks at 80 m (blue lines) were also identified at 100 m (red lines) where these peaks slightly shifted in northern direction due to the mean wind vector. The turbulent eddies were transported by the horizontal wind, which had a speed of between 3 and 7 m s^{-1} and wind direction from the south (150 to 180°). The measurements at 80 m and 100 m showed repeated (or persistent) high peaks that were observed at the same position within a 6-h time interval (Fig. 7a, c, e). This indicates that the enhanced turbulent activity was likely due to differences in the underlying surface characteristics.

The surface beneath the flight path was heterogeneous and consisted of patches of forest, grassland, farmland and built-up area. In the northern part, from latitude 52.19° on, also scattered buildings were present that probably caused the peaks in C_T^2 at this latitude. In the middle of the flight path the M^2AV first crossed a road with trees (52.174°) followed by patches of forest (between 52.175° and 52.179°) that could have induced additional turbulence due to the change in surface roughness and different thermal properties.

5.3.1 Averaged Spatial Series of C_T^2

To verify the effect of the heterogeneous surface, the variations in time were reduced by averaging the spatial series of C_T^2. Only the legs of 5.6-km length, flown along the scintillometer path were used to cover the largest possible distance (see Table 2). The individual C_T^2 spatial series were normalized with their spatially-averaged value, $\overline{C_T^2}$, and defined as a normalized spatial series:

$$\widetilde{C_T^2}_i = \frac{C_{T\,i}^2}{\overline{C_T^2}}, \tag{13}$$

at data point i.

All normalized spatial series were then averaged and the result is shown in Fig. 8. The coloured areas represent the standard deviation of the averaged $\widetilde{C_T^2}$ for each data point i,

$$\sigma\left(\widetilde{C_T^2}\right)_i = \sqrt{\frac{1}{n}\sum_{j=1}^{n}\left(\langle\widetilde{C_T^2}\rangle_i - \widetilde{C_T^2}_{j,i}\right)^2}, \tag{14}$$

where n is the number of flight legs and the brackets $\langle\ \rangle$ represent the average of $\widetilde{C_T^2}$ over all legs j at data point i.

Three lines are shown in Fig. 8, representing the averaged spatial series for the first day, the second day and for both days together. The average for the first day was based on 12 legs flown between 0742 and 1430 and showed the largest peak in the middle of the path. The second day average was based on 20 legs flown between 0613 and 1613 and showed the same

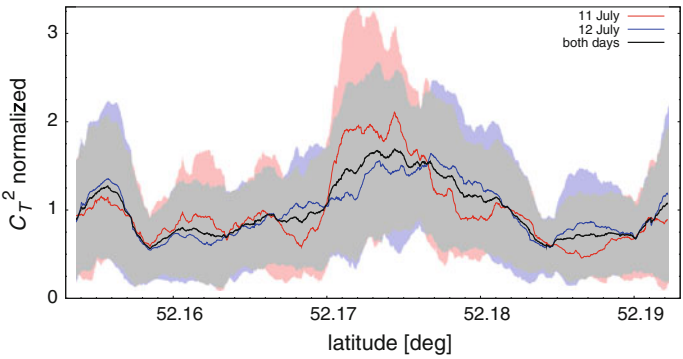

Fig. 8 The averaged spatial series of the normalised C_T^2 for 11 July (three flights between 0742 and 1430) represented by the *red line*, 12 July (5 flights between 0613 and 1613) represented by the *blue line* and for both days represented by the *black line*. The *red*, *blue* and *grey filled areas* represent the standard deviations of the corresponding curves (see Eq. 14)

behaviour along the path compared to the first day. The black line represents the average for all 32 legs measured on both flight days. The standard deviations were relatively large but still an obvious signature of the variability along the flight-path was visible. When flying from south towards north, first a small peak occurred at 52.156° followed by a decrease and a slight increase of the normalised C_T^2 toward the second maximum. The second significant peak occurs at a latitude of 52.174° with a maximum of 1.7 times the mean C_T^2 value. Flying further in northern direction, the normalized C_T^2 decreases until 52.185° followed by a small increase again at the northern end of the flight path. Particularly, the peak in the middle of the flight path indicates the influence of the surface. However, without near-surface reference measurements it cannot be decided where this peak is attributed to, e.g. the patches of forest, at the sudden change of the farmland type at 52.172°.

5.4 Vertical Profiles

Within the lower convective boundary layer, the height dependence of the temperature structure parameter was described as Wyngaard et al. (1971) as

$$C_T^2 = Az^{-4/3}, \tag{15}$$

with the variable A that includes information on the temperature and the surface heat flux. To prove this dependency, the vertical profiles measured during daytime are shown in Figs. 9 and 10. For the late afternoon (1700–1800) no vertical profiles were shown since the measured C_T^2 were very low (see Appendix Tables 3, 4) and no significant height dependency could be found during the evening transition. In Figs. 9 and 10, the fit (dashed line) represents (Eq. 15), which was applied on the M^2AV data only (using a least-squares procedure). The sonic data are additionally plotted for comparison (red symbols) but were not included in the approximation of Eq. 15. Although the box patterns were flown over a different surface compared to the longer legs, the mean C_T^2 measured along these short legs fitted well to the other data. For the morning flights on both days (0613–0816) the scaling (15) applied well. For these flights, the deviation of C_T^2 from the fitted line was less than 50% of the measured C_T^2 value. The sonic data at 90 m also agreed well with the aircraft profile at these times. For the following flights (1050–1430) the variability between the C_T^2 values at 60 m increased, which made it difficult to define an accurate height dependency. Around this time the turbulent

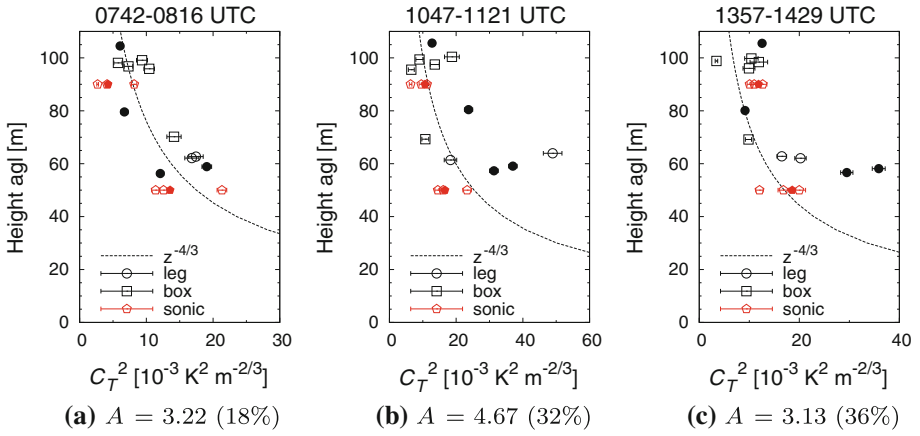

Fig. 9 July 11, 2010. Vertical profiles of C_T^2 measured by M^{2}AV (*black squares* and *circles*) and the sonics (*red pentagons*). The *closed black symbols* represent the long flights of 5.6 km length. The *open red pentagons* represent the 10-min sonic data and the *closed red pentagons* represent the 30-min sonic data. The *dashed lines* represent the fit ($Az^{-4/3}$) through the M^{2}AV data only. The individual captions of the sub figures give the value of A and the root-mean-square error of the fit within the parentheses

eddies were large and intense with also large temporal fluctuations, causing a very unsteady convective flow that made it hard to measure a C_T^2 profile without large variations.

Except for the morning flights, the sonic measurements at 50 m were slightly smaller compared to the UAV values in 60 m. The difference between both systems was probably due to the different C_T^2 footprints. The effect of these different footprints was most pronounced around noon and in the lower heights where the influence of the different surface types was largest. The vertical profiles measured on the second day in the late afternoon (Fig. 10e) met the scaling nicely and also showed less variations in C_T^2 between the flight legs in one height. The parameter A varied between 1.06 and 5.19, depending on the time of day, with a maximum around 1100 UTC. The magnitudes of A were slightly higher on the second day due to the higher C_T^2 values.

6 Conclusions and Outlook

We showed that the automatically operating research UAV, M^{2}AV, was able to measure the spatially-averaged temperature structure parameter C_T^2 in the daytime convective ABL during two summer days at different heights above a heterogeneous land surface (with respect to land use). Additionally, the air temperatures measured by two sonic anemometers were used to compute the temporally averaged C_T^2. Both systems showed a pronounced diurnal cycle of C_T^2 with an increase after sunrise, the highest values around noon and a decrease towards sunset. This behaviour was most obvious for the lowest levels (50, 60 m above the ground), but it was also present at 100 m. Although both systems have different sampling characteristics and slightly different C_T^2 footprints, the derived values were of the same order of magnitude. The variability of the M^{2}AV C_T^2 values between the flight legs at one height was largest around midday. This variation is attributed to the structure of turbulence varying both in space and time. It appears to be difficult to separate temporal variability from spatial variability (the latter being possibly related to surface heterogeneity and therefore time invariant) from only four flight legs. A larger number of flight legs might be needed to obtain

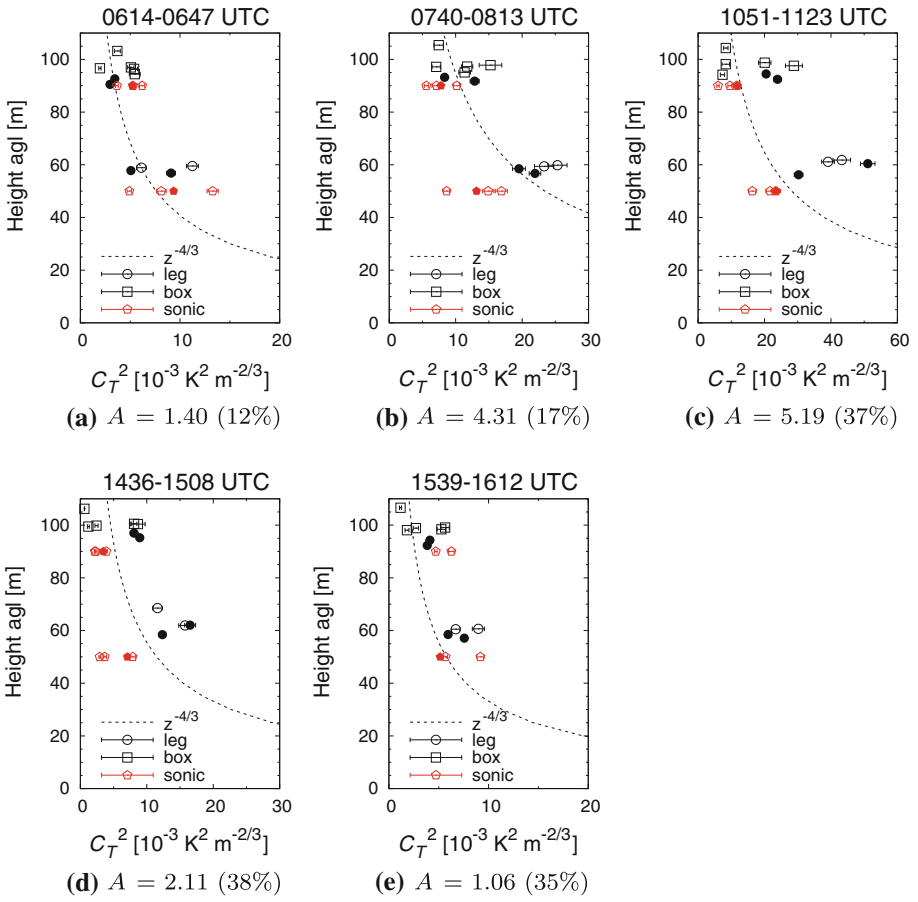

Fig. 10 Same as Fig. 9, but for July 12, 2010

a more stable ensemble average. The 10-min averages of the sonic data showed considerable variation in time as well, which was of the same order of magnitude as the differences between the individual M^{2}AV flight legs.

The spatial series of C_T^2 measured by the M^{2}AV showed the variability of the temperature structure parameter along the flight path. It was observed that maxima of C_T^2 remained or recurred at the same position along the flight path during the different flights. The average of the normalized C_T^2 of 32 legs showed a clear signature of the C_T^2 variability along the flight path. In the middle of the path a significant increase of C_T^2 was observed that was found to be coupled to the surface heterogeneity. For future campaigns a camera and a laser altimeter should be implemented aboard the aircraft to observe the surface type and scan the real height above the surface so that information on the roughness could be obtained.

The temperature structure parameter showed the expected decrease with height for all cases except one. During the early morning flight of 11 July (0505–0538 UTC) C_T^2 increased with height. This flight took place in and above a shallow growing convective boundary layer with the remnants of a nocturnal LLJ in the stable layer aloft. Strong wind shear below this low-level wind maximum together with entrainment processes at the top of the shallow convective boundary layer resulted in a strong increase of C_T^2 between 80 and 100 m above

the surface. During all the other flights, turbulence was generated at the surface and a decrease of C_T^2 with height was found. However, the height scaling $C_T^2 \sim z^{-4/3}$ could be applied for the morning (0614–0816 UTC) and late afternoon (1540–1615 UTC) flights only. During the flights around midday (1047–1510 UTC) the variations of the derived structure parameters at the lowest flight levels were too large to apply a proper fit. This may indicate a deficit in adequately sampling all relevant scales within the deep noontime convective ABL. For the late afternoon flights (from 1700 UTC on), turbulence started to decay and the C_T^2 values were very low with no significant height dependency.

The application of small automatically operating UAV in boundary-layer meteorology shows very promising results. Two of the authors recently moved from TU Braunschweig to Tübingen University where the development of a new research UAV (MASC: multi-purpose automatic sensor carrier, 2 m wing span, 5 kg maximum weight including 1.5 kg scientific payload) is near completion (December 2010). The new UAV will be able to operate one hour in wind speeds up to 15 m s^{-1} and to carry a laser altimeter, a camera and (in addition to fast wind and temperature sensors) a fast humidity sensor. The latter will allow for the measurement of the humidity structure parameter C_Q^2. The new aircraft with enhanced capabilities of performing fast-response turbulence measurements in the ABL will be operated in the Lindenberg area again during a second field experiment on structure parameters along a scintillometer path. This experiment is planned for 2012, where we plan to derive the full set of structure parameters according to (1) (i.e., C_T^2, C_Q^2 and C_{TQ}) from airborne measurements. These data shall then be analyzed in relation to scintillometer measurements from a combination of optical and microwave scintillometry.

Acknowledgments We are much obliged to both anonymous reviewers whose reviews highly improved the final paper. The data analysis is funded by the German Science Foundation DFG (Turbulent structure parameters over heterogeneous terrain—implications for the interpretation of scintillometer data, Grant Ba 1988/9-1 and Be 2044/3-1).

Appendix

Table 3 The spatially-averaged C_T^2 (10^{-3} K^2 $m^{-2/3}$) measured by the M^2AV on July 11, during the five flights (time periods, UTC)

Flight-section	Distance (km)	z (m)	0504–0539	0742–0816	1047–1122	1356–1430	1722–1756
leg01sn	3.3	60	3.0 (0.2)	17.4 (1.1)	18.3 (1.9)	16.5 (1.0)	0.7 (0.0)
leg01ns	5.6	60	2.6 (0.1)	19.1 (0.7)	37.0 (1.3)	35.9 (1.3)	1.1 (0.1)
leg02sn	5.6	80	3.8 (0.2)	6.7 (0.6)	23.7 (1.2)	9.1 (0.5)	0.8 (0.0)
leg02ns	5.6	100	16.5 (0.6)	6.1 (0.3)	12.8 (0.7)	12.6 (0.6)	1.0 (0.0)
box03ns	2.0	100	15.2 (0.7)	10.4 (0.8)	6.6 (0.9)	9.9 (1.2)	1.4 (0.1)
box03we	2.0	100	18.7 (1.2)	9.3 (0.8)	18.7 (2.2)	3.4 (0.3)	0.6 (0.0)
box03sn	2.0	100	12.5 (0.6)	5.7 (0.6)	9.0 (1.1)	10.4 (1.3)	0.3 (0.0)
box03ew	2.0	100	12.3 (1.1)	7.3 (0.6)	13.6 (1.3)	11.9 (1.8)	0.2 (0.0)
leg04sn	3.3	60	3.3 (0.2)	16.8 (1.1)	48.9 (2.8)	20.2 (1.1)	0.6 (0.0)
leg04ns	5.6	60	3.1 (0.1)	12.1 (0.5)	31.3 (1.3)	29.5 (1.2)	0.6 (0.0)
box05sn	2.0	70	3.5 (0.2)	14.1 (1.1)	10.8 (1.0)	9.8 (0.6)	–

The values in parentheses represent the standard error of C_T^2 according to (12)

Table 4 The spatially-averaged C_T^2 (10^{-3} K^2 m$^{-2/3}$) measured by the M^{2}AV on July 12, during the six flights (time periods, UTC)

Flight-section	z (m)	0613–0647	0739–0814	1050–1124	1435–1509	1538–1613	1707–1742
leg01sn	60	6.1 (0.5)	25.3 (1.4)	43.3 (2.6)	11.6 (0.7)	9.0 (0.6)	0.8 (0.0)
leg01ns	60	5.1 (0.3)	19.5 (1.0)	51.1 (2.2)	16.5 (0.8)	5.9 (0.3)	0.7 (0.0)
leg02sn	90	3.0 (0.2)	12.9 (0.7)	23.9 (1.1)	8.9 (0.5)	3.8 (0.2)	0.2 (0.0)
leg02ns	90	3.5 (0.2)	8.3 (0.4)	20.5 (0.9)	8.1 (0.6)	4.1 (0.2)	0.4 (0.0)
box03ns	100	3.7 (0.3)	7.4 (0.7)	8.3 (0.7)	0.6 (0.0)	1.2 (0.1)	0.5 (0.0)
box03we	100	5.4 (0.3)	15.2 (1.7)	8.3 (1.2)	1.2 (0.1)	5.6 (0.4)	0.6 (0.0)
box03sn	100	5.1 (0.3)	11.7 (0.8)	20.1 (1.9)	8.1 (0.4)	2.7 (0.3)	0.3 (0.0)
box03ew	100	5.5 (0.5)	11.3 (0.9)	28.9 (2.5)	8.7 (1.1)	5.3 (0.4)	0.2 (0.0)
leg04sn	60	11.2 (0.6)	23.3 (1.4)	39.1 (1.9)	15.7 (0.9)	6.7 (0.4)	0.5 (0.0)
leg04ns	60	9.1 (0.4)	21.9 (0.9)	30.3 (1.3)	12.3 (0.5)	7.6 (0.3)	1.3 (0.0)
box05sn	100	2.0 (0.1)	7.1 (0.6)	7.3 (0.6)	2.4 (0.2)	1.8 (0.2)	0.7 (0.1)

The values in parentheses represent the standard error of C_T^2 (12)

References

Bange J, Spieß T, van den Kroonenberg AC (2007) Characteristics of the early-morning shallow convective boundary layer from helipod flights during STINHO-2. Theor Appl Climatol 90(1–2):113–126

Banta R, Newsom R, Lundquist J, Pichugina Y, Coulter R, Mahrt L (2002) Nocturnal low-level jet characteristics over Kansas during CASES-99. Boundary-Layer Meteorol 105:221–252

Beyrich F, Mengelkamp HT (2006) Evaporation over a heterogeneous land surface: EVA_GRIPS and the LITFASS-2003 experiment—an overview. Boundary-Layer Meteorol 121:1–28

Beyrich F, de Bruin HAR, Meijninger WML, Schipper JW, Lohse H (2002) Results from one-year continuous operation of a large aperture scintillometer over a heterogeneous land surface. Boundary-Layer Meteorol 105:85–97

Braam M (2010) Determination of the surface sensible heat flux from the structure parameter of temperature at 60 m height during day-time. KNMI technical report TR-303, 39 pp

Bromba MUA, Zlegler H (1981) Application hints for Savitzky-Golay digital smoothing filters. Anal Chem 53:1583–1586

Coulman CE (1973) Vertical profiles of small-scale temperature structure in the atmosphere. Boundary-Layer Meteorol 4:169–177

Cuijpers JWM, Kohsiek W (1989) Vertical profiles of the structure parameter of temperature in the stable, nocturnal boundary layer. Boundary-Layer Meteorol 47:111–129

Cuxart J (2008) Nocturnal basin low-level jets: an integrated study. Acta Geophys 56(1):100–113

Cuxart J, Jiménez MA (2007) Mixing processes in a nocturnal low-level jet: an LES study. J Atmos Sci 64:1666–1679

de Bruin HAR, van den Hurk BJJM, Kohsiek W (1995) The scintillation method tested over a dry vineyard area. Boundary-Layer Meteorol 76:25–40

Fairall CW (1987) A top-down and bottom-up diffusion model of C_T^2 and C_q^2 in the entraining convective boundary layer. J Atmos Sci 44:1009–1017

Fairall CW, Markson R, Schacher GE, Davidson KL (1980) An aircraft study of turbulence dissipation rate and temperature structure function in the unstable marine atmospheric boundary layer. Boundary-Layer Meteorol 19:453–469

Frisch AS, Clifford SF (1975) A note on the behaviour of the temperature structure parameter in a convective layer capped by a marine inversion. J Appl Meteorol 14:415–419

Görsdorf U, Adedokoun JA, Engelbart DAM (2004) Low-level jet climatology using combined sodar and wind profiler measurements. In: Proceedings of the 12th international symposium on acoustic remote sensing, Cambridge, UK

Hoedjes JCB, Chehbouni A, Ezzahar J, Escadafal R, de Bruin HAR (2007) Comparison of large aperture scintillometer and eddy covariance measurements: can thermal infrared data be used to capture footprint-induced differences? J Hydrometeorol 8:144–159

Holland GJ, Webster PJ, Curry JA, Tyrell G, Gauntlett D, Brett G, Becker J, Hoag R, Vaglienti W (2001) The Aerosonde robotic aircraft: a new paradigm for environmental observations. Bull Am Meteorol Soc 82(5):889–901

Kaimal JC, Finnigan JJ (1994) Atmospheric boundary layer flows—their structure and measurement. Oxford University Press, New York, 289 pp

Kaimal JC, Gaynor JE (1991) Another look to sonic thermometry. Boundary-Layer Meteorol 56:401–410

Kohsiek W (1982) Measuring C_T^2, C_Q^2, and C_{TQ} in the unstable surface layer, and relations to the vertical fluxes of heat and moisture. Boundary-Layer Meteorol 24:89–107

Kolmogorov A (1941) Local structure of turbulence in an incompressible fluid for very large Reynolds numbers. Dokl Akad Nauk SSSR 30:299–303

Lenschow DH, Stankov BB (1986) Length scales in the convective boundary layer. J Atmos Sci 43:1198–1209

Lenschow DH, Mann J, Kristensen L (1994) How long is long enough when measuring fluxes and other turbulence statistics. J Atmos Ocean Technol 11:661–673

Lumley L, Panofsky H (1964) The structure of atmospheric turbulence. Wiley, New York, 239 pp

Ma S, Chen H, Wang G, Pan Y, Li Q (2004) A miniature robotic plane meteorological sounding system. Adv Atmos Sci 21:890–896

Martin S, Bange J, Beyrich F (2011) Profiling the lower troposphere using the research UAV 'M^{2}AV Carolo'. Atmos Meas Tech 4:705–716

Mayer S, Sandvik A, Jonassen MO, Reuder J (2010) Atmospheric profiling with the UAS SUMO: a new perspective for the evaluation of fine-scale atmospheric models. Meteorol Atmos Phys 12. doi:10.1007/s00703-010-0063-2

Meijninger WML, de Bruin HAR (2000) The sensible heat fluxes over irrigated areas in western Turkey determined with a large-aperture scintillometer. J Hydrol 229:42–49

Meijninger WML, Beyrich F, Lüdi A, Kohsiek W, de Bruin HAR (2006) Scintillometer-based turbulent fluxes of sensible and latent heat over a heterogeneous land surface—a contribution to LITFASS-2003. Boundary-Layer Meteorol 121:89–110

Nieveen JP, Green AE (1999) Measuring sensible heat flux density over pasture using the C_T^2-profile method. Boundary-Layer Meteorol 91:23–35

Reuder J, Brisset P, Jonassen M, Müller M, Mayer S (2009) The small unmanned meteorological observer SUMO: a new tool for atmospheric boundary layer research. Meteorol Z 18(2):141–147

Rotta JC (1972) Turbulente Strömungen. Eine Einführung in die Theorie und ihre Anwendung. Teubner, Stuttgart

Soddell JR, McGuffie K, Holland GJ (2004) Intercomparison of atmospheric soundings from the Aerosonde and radiosonde. J Appl Meteorol 43:1260–1269

Sorbjan Z (2005) Statistics of scalar fields in the atmospheric boundary layer based on large-eddy simulations. Part I: Free convection. Boundary-Layer Meteorol 116:467–486

Spieß T, Bange J, Buschmann M, Vörsmann P (2007) First application of the meteorological mini-UAV 'M^{2}AV'. Meteorol Z N F 16(2):159–169

Thorpe AJ, Guymer TH (1977) The nocturnal jet. Q J R Meteorol Soc 103:633–653

van den Kroonenberg AC (2009) Airborne measurement of small-scale turbulence with special regard to the polar boundary layer. No. 2009-11 in ZLR-Forschungsbericht, Sierke Verlag, Göttingen, Germany

van den Kroonenberg AC, Spieß T, Buschmann M, Martin T, Anderson PS, Beyrich F, Bange J (2007) Boundary layer measurements with the autonomous mini-UAV M^{2}AV. In: Deutsch - Österreichisch - Schweizerische Meteorologen - Tagung, Deutsche Meteorologische Gesellschaft, Hamburg, Germany, p 10

van den Kroonenberg AC, Martin T, Buschmann M, Bange J, Vörsmann P (2008) Measuring the wind vector using the autonomous mini aerial vehicle M^{2}AV. J Atmos Ocean Technol 25(11):1969–1982

Wyngaard JC, LeMone MA (1980) Behavior of the refractive index structure parameter in the entraining convective boundary layer. J Atmos Sci 37:1573–1585

Wyngaard JC, Izumi Y, Collins SA (1971) Behavior of the refractive-index-structure parameter near the ground. J Opt Soc Am 61:1646–1650

Wyngaard JC, Pennell WT, Lenschow DH, LeMone MA (1978) The temperature-humidity covariance budget in the convectice boundary layer. J Atmos Sci 35:47–58